Comparison of the electronic structures of layered transition-metal trichalcogenides thallium triselenide, thallium trisulfide and niobium triselenide

ARTICLE *in* INORGANIC CHEMISTRY · APRIL 1990

Impact Factor: 4.76 · DOI: 10.1021/ic00332a024

9 AUTHORS, INCLUDING:

Jean-Paul POUGET
Université Paris-Sud 11
316 PUBLICATIONS **6,160** CITATIONS
SEE PROFILE

M-H Whangbo
North Carolina State University
162 PUBLICATIONS **3,089** CITATIONS
SEE PROFILE

Contribution from the Laboratoire de Chimie Théorique (CNRS URA 506) and Laboratoire de Physique des Solides (CNRS LA 2), Université de Paris-Sud, 91405 Orsay, France, Laboratoire de Chimie des Solides, IPCM, Université de Nantes, 44072 Nantes, France, and Department of Chemistry, North Carolina State University, Raleigh, North Carolina 27695-8204

Comparison of the Electronic Structures of Layered Transition-Metal Trichalcogenides $TaSe_3$, TaS_3, and $NbSe_3$

E. Canadell,*,† I. E.-I. Rachidi,† J. P. Pouget,*,‡ P. Gressier,§ A. Meerschaut,§ J. Rouxel,*,§ D. Jung,∥ M. Evain,∥ and M.-H. Whangbo*,∥

Received August 22, 1989

The electronic structures of the three layered transition-metal trichalcogenides $NbSe_3$, TaS_3, and $TaSe_3$ were examined by performing tight-binding band electronic structure calculations. The Fermi surfaces of these materials were also calculated to analyze their metallic and/or charge density wave properties. In these trichalcogenides MX_3 (M = Nb, Ta; X = S, Se) made up of prismatic MX_3 chains, the broken X–X bonds of their equilateral-like MX_3 chains and the short intra- and interlayer X···X contacts are found to be crucial for the semimetallic properties of $TaSe_3$ and for the charge density wave phenomena of $NbSe_3$ and TaS_3. For the electronic parameters of the charge density waves in $NbSe_3$ and TaS_3, a quantitative agreement is obtained between the experimental observations and the present band electronic structure calculations.

Layered transition-metal trichalcogenides MX_3 (M = Nb, Ta; X = S, Se) contain layers made up of trigonal-prismatic chains.[1] These MX_3 prismatic chains are classified as isosceles- or equilateral-like depending upon whether the oxidation state of the X_3 triangle forming the base of the MX_6 prism is $(X^{2-} + X_2^{2-})$ or $3X^{2-}$, respectively.[2] For simplicity, isosceles- and equilateral-like prismatic chains may be referred to as I- and E-prismatic chains, respectively. Thus $NbSe_3$ and monoclinic TaS_3 each have four I- and two E-prismatic MX_3 chains per unit cell, while $TaSe_3$ has two I- and two E-prismatic chains per unit cell. Consequently, it is expected that $NbSe_3$ and TaS_3 each have two d electrons per unit cell but $TaSe_3$ has none. In agreement with this simple electron counting, both $NbSe_3$ and TaS_3 are metals at room temperature. When the temperature is lowered, both undergo two different charge density wave (CDW) transitions. At the end of these two transitions, TaS_3 becomes a semiconductor but $NbSe_3$ remains metallic.[1] The above electron counting on $TaSe_3$ suggests that $TaSe_3$ would be a semiconductor, but it is a semimetal[1]. Although a number of band electronic structure studies on $NbSe_3$[3] and $TaSe_3$[4] have been reported, there has been no systematic study concerning how $NbSe_3$ and TaS_3 differ in their electronic structures and why $TaSe_3$ is semimetallic from the viewpoint of their crystal structures. In addition, Fermi surfaces have not been reported for TaS_3 and $TaSe_3$. Therefore, we carry out tight-binding band electronic structure calculations[5] on $NbSe_3$, TaS_3, and $TaSe_3$ within the framework of the extended Hückel method[6] and discuss similarities and differences in their electronic structures. The atomic parameters employed in our study are summarized in Table I.

Table I. Exponents and Parameters Used in the Calculations

atom	orbital	H_{ii}, eV	ζ_1	ζ_2	c_1[a]	c_2[a]
Nb	5s	−10.10	1.90			
	5p	−6.86	1.85			
	4d	−12.10	4.08	1.64	0.6401	0.5516
Ta	6s	−10.10	2.28			
	6p	−6.86	2.24			
	5d	−12.10	4.76	1.94	0.6597	0.5589
S	3s	−20.00	1.817			
	3p	−13.30	1.817			
Se	4s	−20.50	2.44			
	4p	−13.20	2.07			

[a] Contraction coefficients used in the double-ζ expansion.

Table II. Short X–X and X···X Distances (Å) in $NbSe_3$, TaS_3, and $TaSe_3$ Shown in **1** and **2**

dist	$NbSe_3$	TaS_3	$TaSe_3$
A	2.37	2.07	2.58
A'	2.50	2.11	
B	2.73	2.80	2.66
C	2.92	2.84	2.90
D	3.30	3.26	3.49
E	2.92	2.92	

Crystal Structures and Short X···X Contacts

In the layered trichalcogenide $ZrTe_3$, composed exclusively of I-prismatic chains, short intra- and interlayer Te···Te are found to play a crucial role for its semimetallic property and resistivity anomaly.[7] By analogy, one might expect short X···X contacts of MX_3 (M = Nb, Ta; X = S, Se) to be also important in determining the electronic properties of MX_3. The projection view along the chain direction (i.e., the *b*-axis direction) of $NbSe_3$[8] and

† Laboratoire de Chimie Théorique, Université de Paris-Sud.
‡ Laboratoire de Physique des Solides, Université de Paris-Sud.
§ Université de Nantes.
∥ North Carolina State University.

(1) Reviews: (a) Meerschaut, A.; Rouxel, J. In *Crystal Chemistry and Properties of Materials with Quasi-One-Dimensional Structures*; Rouxel, J., Ed.; Reidel: Dordrecht, The Netherlands, 1986; p 205. (b) Monceau, P. In *Electronic Properties of Inorganic Quasi-One-Dimensional Compounds*; Monceau, P., Ed.; Reidel: Dordrecht, The Netherlands, 1985; Part II, p 139.
(2) Whangbo, M.-H. In *Crystal Chemistry and Properties of Materials with Quasi-One-Dimensional Structures*; Rouxel, J., Ed.; Reidel: Dordrecth, The Netherlands, 1986; p 27.
(3) (a) Shima, N. *J. Phys. Soc. Jpn.* **1982**, *51*, 11; **1983**, *52*, 578. (b) Bullett, D. W. *J. Phys. C: Solid State Phys.* **1982**, *15*, 3069. (c) Whangbo, M.-H.; Gressier, P. *Inorg. Chem.* **1984**, *23*, 1305.
(4) Bullett, D. W. *J. Phys. C: Solid State Phys.* **1979**, *12*, 277.
(5) Whangbo, M.-H.; Hoffmann, R. *J. Am. Chem. Soc.* **1978**, *100*, 6093.
(6) Hoffmann, R. *J. Chem. Phys.* **1963**, *39*, 1397. A modified Wolfsberg–Helmholz formula was used to calculate the off-diagonal H_{ij} values: Ammeter, J. H.; Bürgi, H.-B. Thibeault, J.; Hoffmann, R. *J. Am. Chem. Soc.* **1978**, *100*, 3686.

0020-1669/90/1329-1401$02.50/0

TaS_3[9] is shown by **1**, and that of $TaSe_3$[10] by **2**. It is the type II

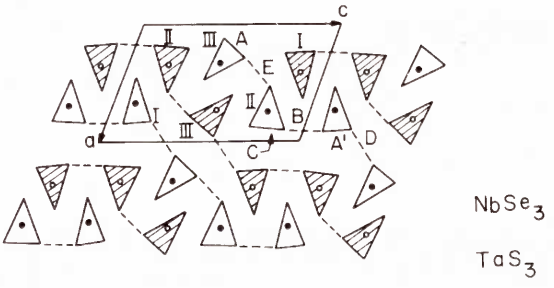

1

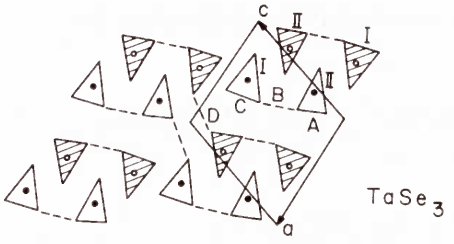

2

chains of **1** and the type I chains of **2** that are E-prismatic chains. Table II summarizes some of the X–X and X···X distances of **1** and **2** that occur among the X atoms with the same *b*-axis height. Clearly, there exist short intra- and interlayer X···X contacts much shorter in length than the van der Waals radii sum (i.e., 3.60 and 3.80 Å for the S···S and Se···Se contacts, respectively[11]). Furthermore, the "broken" X–X bond of an E-prismatic MX_3 chain (i.e., *C* in **1** and **2**) is not really long compared either with the short intralayer X···X contact (i.e., *B* in **1** and **2**) or with the "nonbonded" interlayer X···X contact (i.e., *D* in **1** and **2**). In all the three MX_3 compounds, the MX_3 prismatic chains with the same *b*-axis height are interlinked throughout the lattice by the short intra- and interlayer X···X contacts.

In **2** the broken Se–Se bond (i.e., *C* = 2.90 Å) of each E-prismatic chain has an extremely short Se···Se (i.e., *B* = 2.66 Å) contact wth the Se–Se bond (i.e., *A* = 2.58 Å) of the neighboring I-prismatic chain.[10] Thus the structure of each $TaSe_3$ layer may be described in terms of the four-chain structural unit **3**, quadruple

3 **4**

prismatic chain $(MX_3)_4$, which is made up of a pair of I-prismatic chains flanked with an E-prismatic chain on either side. It is the end Se atom of the broken Se–Se bond in each E-prismatic chain of **3** that is used as a capping atom for the face of the neighboring prismatic chain in assembling a $TaSe_3$ layer [i.e., the $(b, a + c)$ plane] from the quadruple chains **3**. Notice that quadrupole chain units **3** are also present in the $NbSe_3$ and TaS_3 lattice **1**. In each MX_3 layer [i.e., the (b, c) plane] of **1**, the quadruple chain units **3** (made up of type I and type II chains) alternate with the double I-prismatic chain units **4** (made up of type III chains). Alternatively, the lattice **1** may be described in terms of (a, b) sheets of the quadrupole chains that alternate with those of the double chains along the *c* direction. However, the compressibility measurements of $NbSe_3$[12] suggest a stronger bonding along *c* than along *a*.

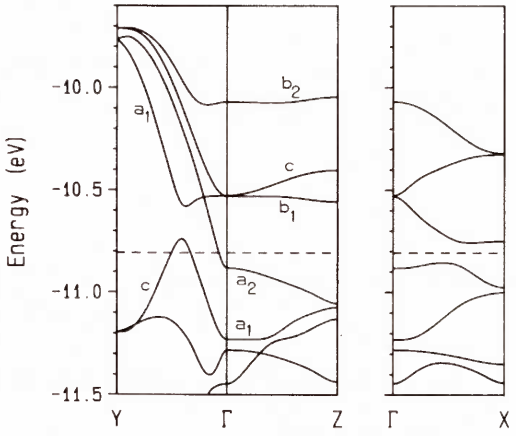

Figure 1. Band electronic structure calculated for the 3D lattice of $TaSe_3$, where the dashed line refers to the Fermi level, $\Gamma = (0, 0, 0)$, $X = (a^*/2, 0, 0)$, $Y = (0, b^*/2, 0)$, and $Z = (0, 0, c^*/2)$.

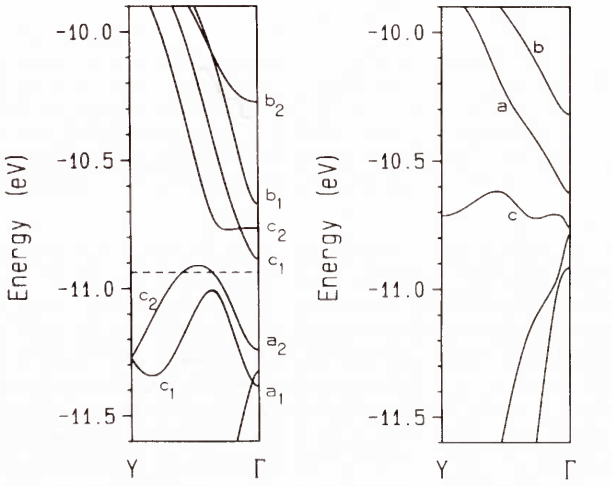

Figure 2. Band electronic structures calculated for (a) the $(b, a + c)$ layer of $TaSe_3$ and (b) the Ta_2Se_8 chain **5**.

Band Dispersions and Fermi Surfaces

A. $TaSe_3$. Band Dispersion. Figure 1 shows the band electronic structure calculated for $TaSe_3$. Bands a_1 and a_2 are essentially derived from the z^2-block orbitals of the I-prismatic chains (i.e., type II chains of **2**),and bands b_1 and b_2 from those of the E-prismatic chains (i.e., type I chains of **2**). Bands a_1 and a_2 are lower in energy than bands b_1 and b_2, because the z^2-block level of the isosceles-like $TaSe_6$ prism lies lower in energy than that of the equilateral-like $TaSe_6$ prism. Band c is largely made up of Se p orbitals, and its top overlaps with the bottom of bands a_1 and a_2, thereby leading to the noncrossing between bands a_1 and c (along $\Gamma \rightarrow Y$) because of symmetry. It is this band overlap that gives rise to the partially filled bands, and hence to the semimetallic properties, of $TaSe_3$.

Origin of the Top p-Block Band. The band electronic structure calculated for a single $(b, a + c)$ $TaSe_3$ layer is shown in Figure 2a, which is essentially the same in character as the corresponding one of three-dimensional (3D) $TaSe_3$ lattice shown in Figure 1. Thus, the occurrence of the Se p-block band top overlapping the d-block band bottom is not caused by the short interlayer Se···Se contacts (e.g., *D* in **2**). To see if the band overlap is due to short

(7) Canadell, E.; Mathey, Y.; Whangbo, M.-H. *J. Am. Chem. Soc.* **1988**, *110*, 104.
(8) (a) Meerschaut, A.; Rouxel, J. *J. Less-Common Met.* **1975**, *39*, 197. (b) Hodeau, J. L.; Marezio, M.; Roucau, C.; Ayroles, R.; Meerschaut, A.; Rouxel, J.; Monceau, P. *J. Phys. C: Solid State Phys.* **1978**, *11*, 4117.
(9) Meerschaut, A.; Guemas, L.; Rouxel, J. *J. Solid State Chem.* **1981**, *36*, 118.
(10) Bjerkelund, E.; Fermor, J. H.; Kjeskshus, A. *Acta Chem. Scand.* **1966**, *20*, 1836.
(11) Bond, A. *J. Phys. Chem.* **1964**, *68*, 441.
(12) Yamaya, K.; Oomi, G. *J. Phys. Soc. Jpn.* **1983**, *52*, 1886.

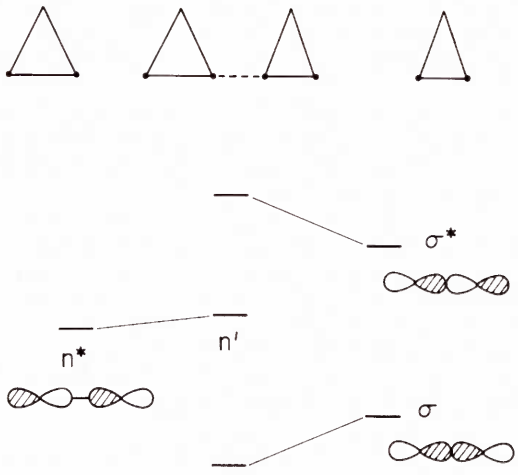

Figure 3. Interaction of the n* level of the broken X–X bond with the σ and σ^* levels of the unbroken X–X bond via the short X···X contact in the quadruple chain unit **3**.

intralayer Se···Se contacts, we calculate the band electronic structure of Ta_2Se_8 chain **5** (i.e., I- and E-prismatic chains plus

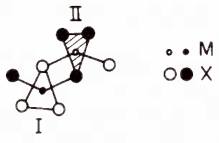

5

two capping Se atoms). As shown in Figure 2b, chain **5** has flat band c just below the z^2-block bands a and b (representing the I- and E-prismatic chains, respectively). Band c is mainly given by the Se p orbitals of the broken Se–Se bond of the E-prismatic chain and is the highest lying Se p-block band. The broken X–X bond of an E-prismatic chain has a nonbonding level n*, which originates from the σ^* level of the bond before breaking. Essentially, the overlap of the Se p-block band top with the d-block bottom in $TaSe_3$ is possible because the n* level is high in energy due to the fact that the broken X–X bond is not long enough to reduce all the σ^* character.

As noted earlier, the broken X–X bond of an E-prismatic chain has a short X···X contact with the X–X bond of the neighboring I-prismatic chain (see **3**). We now consider how the n* level of the broken X–X bond is affected by the short X···X contact. In the quadruple chain unit **3**, the n* level of each E-prismatic chain interacts with the σ and σ^* levels of the X–X bond of the neighboring I-prismatic chain. As schematically shown in Figure 3, the n* level lies in between the σ and σ^* levels, so that n* is raised in energy by σ but lowered in energy by σ^*. As a result, the resulting level n′, which is the major orbital component of the top p-block band in a $TaSe_3$ layer and 3D $TaSe_3$ lattice, is not significantly different in energy from n*. Although there exist intralayer Se···Se interactions, the semimetallic band overlap of $TaSe_3$ originates primarily from the fact that the n* level of the E-prismatic chain is high in energy. However, in terms of orbital character, the n′ level is delocalized in the X–X···X–X units of the quadruple chain **3**, as illustrated in **6**. Namely, the I- and

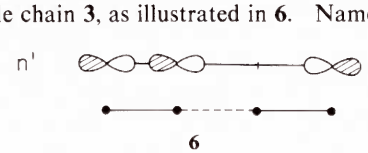

6

E-prismatic chains of **3** are strongly coupled to one another, so that the quadruple chain **3** is an integral structural building unit.

Fermi Surface. Parts a and b of Figure 4 show stereodiagrams of the Fermi surfaces associated with the lower and upper partially filled bands of Figure 1, respectively. The lower band is slightly empty near the top, while the upper one is slightly filled near the bottom. Thus, the lower and upper partially filled bands lead to

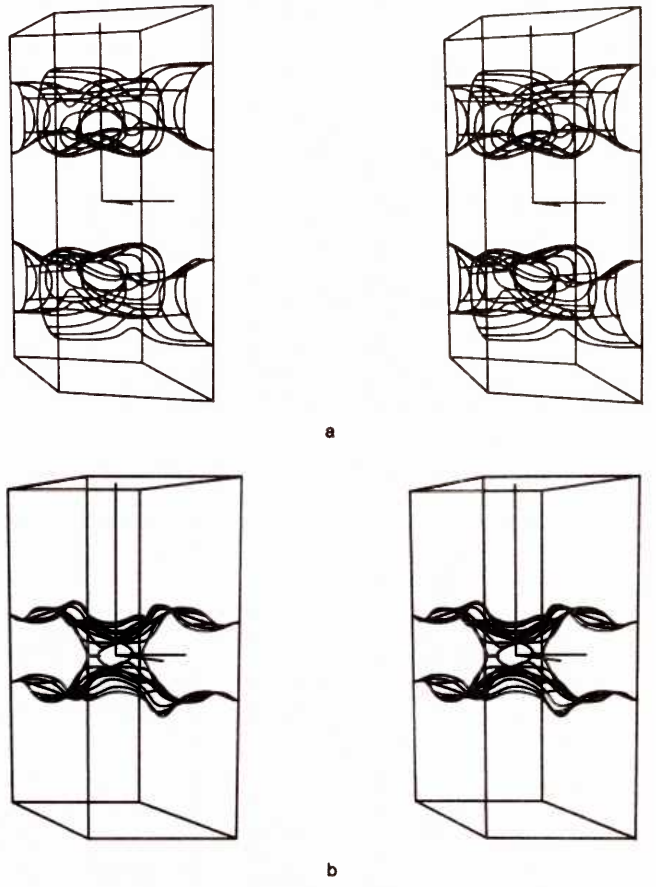

Figure 4. Fermi surfaces of $TaSe_3$ calculated for (a) the lower- and (b) the upper-lying partially filled bands of Figure 1. They represent the hole and the electron pockets, respectively. The a^*, b^*, and c^* axes form a right-handed coordinate system, and the b^* axis corresponds to the vertical axis.

a hole and an electron Fermi surface, respectively. The hole Fermi surface of Figure 4a can be described as fused tunnels running along the $(-a^* + c^*)$ direction, i.e., perpendicular to the layer. The electron Fermi surface of Figure 4b is derived from planes parallel to the b^* axis (i.e., the chain direction) by merging them at certain intervals along the $(-a^* + c^*)$ direction, so that this surface also has a feature of fused tunnels running perpendicular to the layer. These results are in agreement with the experimental deduction,[13,14] from the angular dependence of Shubnikov–de Haas orbits, that the Fermi surface of $TaSe_3$ has cylindrical elements with an axis perpendicular to the layer. The tunnellike Fermi surfaces perpendicular to the layer mean that intrachain and intralayer interactions are stronger than interlayer interactions. However, the latter are not negligible since the tunnel fusing is not possible without them. Although the main features of the Fermi surfaces can be understood by the above arguments, Figure 4 shows that its shape is relatively complex. Thus, a large number of "neck" and "belly" orbits are expected from the Fermi surface, in agreement with the Shubnikov–de Haas data.[14]

B. $NbSe_3$ and TaS_3. Band Dispersion. The band electronic structures of $NbSe_3$ and TaS_3 are shown in Figures 5 and 6, respectively. Let us first consider the band dispersion relations along the chain direction $\Gamma \rightarrow Y$. As shown in **1**, both $NbSe_3$ and TaS_3 have four I- and two E-prismatic chains per unit cell. Thus, the two z^2-block bands (b_1 and b_2) of the E-prismatic chains lie higher in energy than the four z^2-block bands (labeled as a for simplicity) of the I-prismatic chains. At Γ, the bottom of band b_1 is closer to bands a in $NbSe_3$ than in TaS_3. In both $NbSe_3$ and TaS_3, the d-block band bottom overlaps with the chalcogen

(13) Wilson, J. A. *Phys. Rev. B* **1979**, *19*, 6456.
(14) Fleming, R. M.; Polo, J. A.; Coleman, R. V. *Phys. Rev. B* **1978**, *17*, 1634.

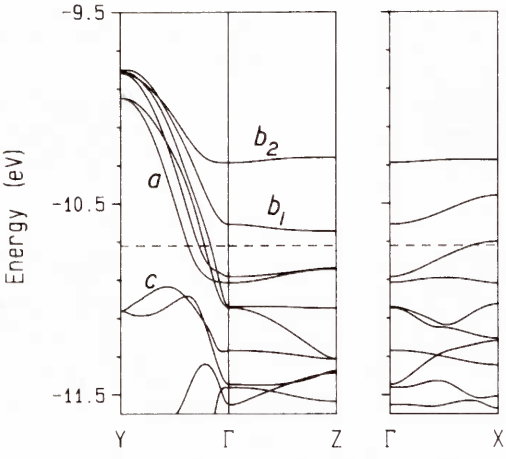

Figure 5. Band electronic structure calculated for $NbSe_3$.

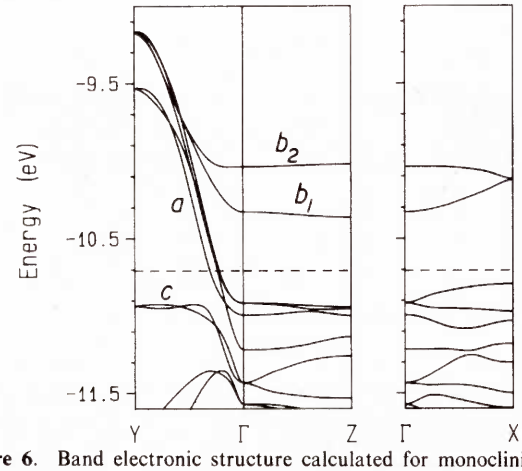

Figure 6. Band electronic structure calculated for monoclinic TaS_3.

p-block band top, which is essentially derived from the n′ levels of the quadruple chain units of the lattice (see Figure 4). This situation is virtually identical with that observed for $TaSe_3$ in the previous section. In contrast to the case of $TaSe_3$, however, $NbSe_3$ and TaS_3 each have nonzero (i.e., two) d electrons per unit cell so that the bottom four of the six z^2-block bands (i.e., bands a) become partially filled. In our calculations, band b_1 of $NbSe_3$ lies slightly above the Fermi level at Γ, in agreement with the previous study of Whangbo and Gressier.[3c] In other band calculations by Bullett[3b] and by Shima,[3a] band b_1 slightly dips below the Fermi level at Γ. This difference is caused by a small change in the relative band energy of the order of 0.1 eV. This minor difference is not of our concern, since we are primarily interested in the relationships between the Fermi surfaces and the CDW instabilities, which are associated with chains I and III according to ^{93}Nb NMR measurements on $NbSe_3$.[15] The CDW's of $NbSe_3$ are similar in character to those of TaS_3,[1] for which band b_1 lies considerably higher in energy from the Fermi level. Thus, it is quite clear that the bottom four z^2-block bands are responsible for the CDW instabilities of the the materials. Two of these four bands are primarily represented by the z^2-block levels of type III chains, and the other two by those type I chains. Namely, the z^2-block bands of type III chains do not strongly interact with those of type I chains. This originates from the crystal structure of MX_3, in which quadruple chains **3** are separated by double chains **4** in each MX_3 (*b*, *c*) layer, and also from the z^2-block orbital of each MX_6 prism, which extends mainly toward the chain direction. Along $\Gamma \rightarrow Y$ the four partially filled bands are split more strongly in $NbSe_3$ than in TaS_3, which reflects the fact that intrachain interactions in either the type I or the type III pair are stronger in $NbSe_3$. In Figure 5, the four partially filled z^2-block bands near the Fermi level have the character of type I, III, III, and I chains on going from Γ to *Y*, respectively, as already pointed out earlier.[3c] This finding reflects the fact that intrachain interactions are stronger in the type I than in the type III pair, which is also the case for TaS_3. Finally, we note that the four partially filled z^2-block bands have a slightly stronger dispersion in TaS_3 than in $NbSe_3$ (~2.0 vs 1.5 eV).

In both $NbSe_3$ and TaS_3, band c is derived mainly from the n′ levels of the quadruple chain units, as described earlier (see **3** and **6**). This band is more dispersive along $\Gamma \rightarrow X$ (i.e., interlayer direction) than along $\Gamma \rightarrow Z$. This results from the way the n′ levels, which represent the X–X···X–X units of the quadruple chains (see **3** and **6**), interact via the short interlayer X···X contacts (i.e., *D* in **1**). In both $\Gamma \rightarrow X$ and $\Gamma \rightarrow Z$ directions, band c is more dispersive for $NbSe_3$ than for TaS_3. This is a consequence of the fact that the MX_3 chains with the same *b*-axis height are interlinked throughout the lattice by the short intra- and interlayer X···X contacts (*E* and *D*, respectively, in **1**). As listed in Table II, these short X···X contacts are comparable in length in $NbSe_3$ and TaS_3. Therefore, the Se···Se contacts provide better overlap than do the S···S contacts since Se has more diffuse atomic orbitals than S. This is why, along $\Gamma \rightarrow X$, band c crosses the Fermi level in $NbSe_3$ but remains below the Fermi level in TaS_3. Thus, the electronic structure of TaS_3 at the Fermi level is one-dimensional (1D), while that of $NbSe_3$ can present some features that are more than 1D in character.

It is clear from Figures 5 and 6 that the Fermi level of $NbSe_3$ and TaS_3 occurs slightly above the energy region where the chalcogen p-block band top overlaps with the z^2-block band bottom. Consequently, the z^2-block bands would acquire some chalcogen p-block band character. This is particularly true for the two z^2-block bands representing type I chains, because these chains are a part of the quadruple chains whose n′ levels form the major orbital component of the chalcogen p-block band top (i.e., band c in Figures 5 and 6). Consequently, of the four partially filled z^2-block bands, the two representing type I chains should have Fermi surfaces that deviate more from the ideal 1D shape (i.e., perfect plane perpendicular to the chain direction).

Fermi Surfaces and CDW Instabilities. When the temperature is lowered, $NbSe_3$ and TaS_3 exhibit two independent 3D CDW orderings, which occur at different temperatures.[1] In $NbSe_3$ the first CDW ordering with the wave vector $\mathbf{q}_1 = (0, 0.241, 0)$ occurs below $T_1 = 145$ K, while the second CDW ordering with the wave vector $\mathbf{q}_2 = (0.5, 0.259, 0.5)$ occurs below $T_2 = 59$ K. The corresponding values for TaS_3 are $\mathbf{q}_1 = (0, 0.254, 0)$ and $T_1 = 240$ K for the first CDW ordering and $\mathbf{q}_2 = (0.5, 0.245, 0.5)$ and $T_2 = 160$ K for the second CDW ordering. These 3D CDW orderings give rise to superlattice spots in X-ray or electron diffraction measurements. Above a 3D CDW ordering temperature, there exists a temperature regime characterized by 1D CDW fluctuations (i.e., pretransitional CDW fluctuation), which give rise to diffuse lines (at the distance of $\pm 2\mathbf{k}_F$ from layers of Bragg spots perpendicular to the 1D direction; $\mathbf{k}_F$ is the Fermi wave vector of the 1D system) in X-ray or electron diffraction patterns.[16] (Each diffuse line in fact represents the intersection of a diffuse sheet with the Ewald sphere of the reciprocal space in which diffraction measurements are described.) In both $NbSe_3$[17] and TaS_3,[18] two types of diffuse lines corresponding to $\mathbf{q}_1$ and $\mathbf{q}_2$ are observed up to room temperature. To relate these observations to the electronic structures, we calculate the Fermi surfaces associated with the partially filled bands of Figures 6 and 7. Stereodiagrams of the four Fermi surfaces for $NbSe_3$ are shown in Figure 7, and those for TaS_3 in Figure 8.

(15) (a) Devreux, F. *J. Phys.* (*Les Ulis, Fr.*) **1982**, *43*, 1489. (b) Ross, J. H., Jr.; Wang, Z.; Slichter, C. P. *Phys. Rev. Lett.* **1986**, *56*, 633.

(16) Moret, R.; Pouget, J. P. In *Crystal Chemistry and Properties of Materials with Quasi-One-Dimensional Structures*; Rouxel, J., Ed.; Reidel: Dordrecht, The Netherlands, 1986; p 87.

(17) Pouget, J. P.; Moret, R.; Meerschaut, A.; Guemas, L.; Rouxel, J. *J. Phys.* (*Les Ulis, Fr.*) **1983**, *44*, C3-1729.

(18) (a) Roucau, C.; Ayroles, R.; Monceau, P.; Guemas, L.; Meerschaut, A.; Rouxel, J. *Phys. Status Solidi A* **1980**, *62*, 483. (b) Moret, R. Unpublished results.

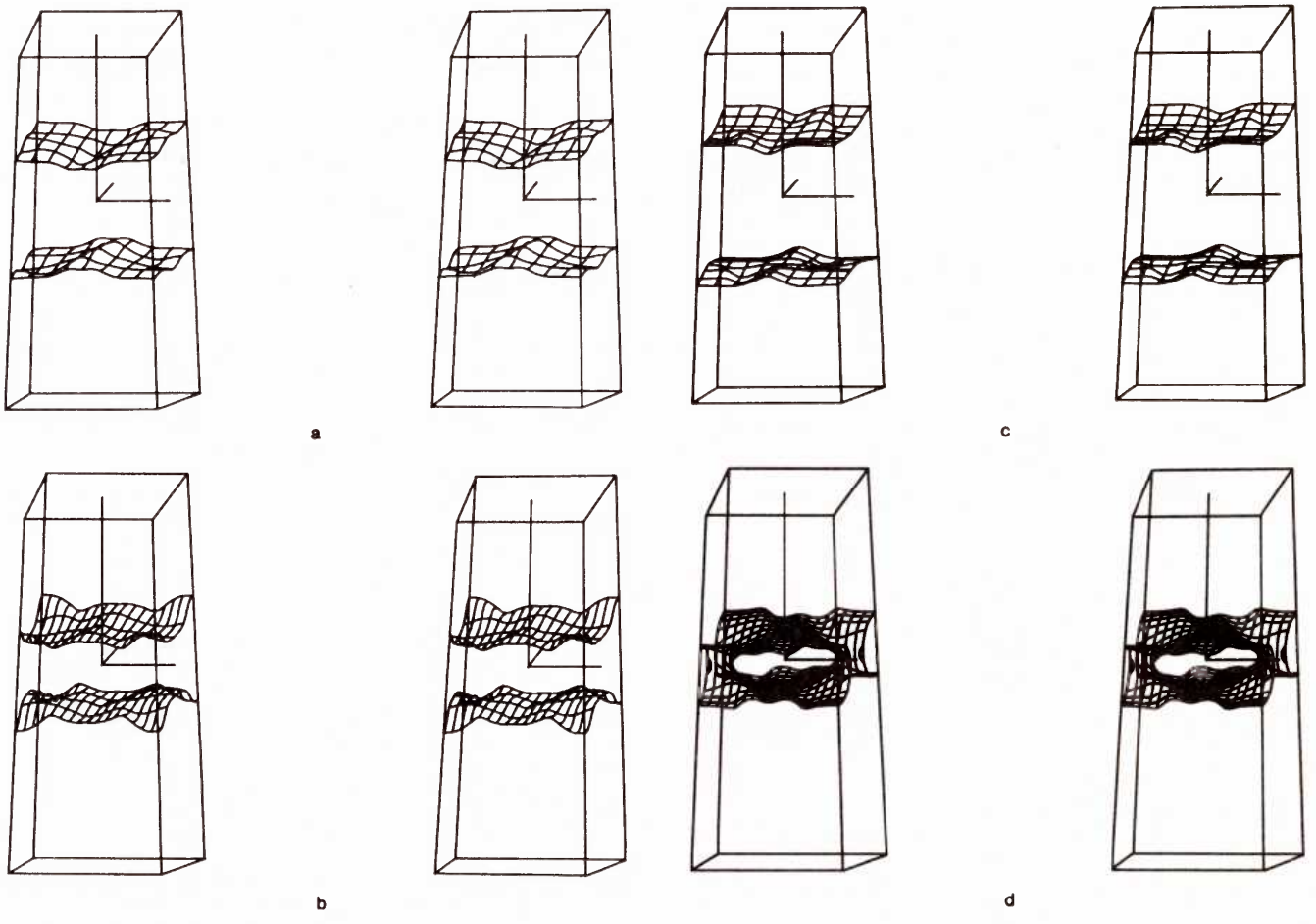

Figure 7. Fermi surfaces of $NbSe_3$ calculated for the (a) second, (b) third, (c) first, and (d) fourth partially filled bands of Figure 5 (on going from Y to Γ at the Fermi level). The a^*, b^*, and c^* axes form a right-handed coordinate system, and the b^* axis corresponds to the vertical axis.

As anticipated from the previous section, the Fermi surfaces of TaS_3 are all open and quasi-planar (1D in nature), and they are flatter than those of $NbSe_3$. Three Fermi surfaces of $NbSe_3$ are also open (quasi-1D in nature). The fourth one (Figure 7d) presents closed portions in the (a^*, b^*) plane and hence a tunnellike shape running along the c^* direction. This is caused by the fact that the Fermi level crosses band c along the $\Gamma \rightarrow X$ direction (see Figure 5). However, the tunnel shape has flat portions perpendicular to the b^* direction. The observation of 1D pretransitional CDW fluctuations in TaS_3 and $NbSe_3$ must be related to the quasi-planar nature of these Fermi surfaces. Since there are four partially filled bands, there are inter- and intraband Fermi surface nestings to consider.[19] In an interband nesting between two partially filled 1D bands, one nesting vector relates their four Fermi surface pieces. In an intraband nesting of one partially filled band, one nesting vector relates its two Fermi surface pieces. Consequently, an interband nesting process is the simplest one that leads to the opening of band gaps in four different bands with only two different CDW nesting vectors in TaS_3 and explains the semiconducting property of TaS_3 below T_2. $NbSe_3$ remains metallic below T_2, and it was estimated that 20% of the total Fermi surface is removed at T_1 while 60% of the remaining Fermi surface is removed at T_2.[20] Occurrence of the same kinds of CDW's in TaS_3 and $NbSe_3$ suggests that the two CDW instabilities of $NbSe_3$ are also caused by interband nesting.

In $NbSe_3$ and TaS_3, two of the four Fermi surfaces are largely derived from type III chains (Figure 7a,b for $NbSe_3$; Figure 8a,b for TaS_3) and the remaining two from type I chains (Figure 7c,d for $NbSe_3$; Figure 8c,d for TaS_3). ^{93}Nb NMR measurements[15]

Table III. Experimental and Theoretical Values of the Physical Parameters Associated with the $\mathbf{q}_1$ and $\mathbf{q}_2$ CDW's of $NbSe_3$ and TaS_3 at Ambient Temperature

	$NbSe_3$		TaS_3	
	$\mathbf{q}_1$	$\mathbf{q}_2$	$\mathbf{q}_1$	$\mathbf{q}_2$
T_c(K)	145	59	240	160
$\xi_\parallel$(Å)	13 ± 4	~10	25 ± 5	~20
ξ_c(Å)	11.5 ± 4	~13	13.2 ± 2.5	~16.5
v_F, 10^{-5} m/s	2.1 ± 0.7	~2.3	2.4 ± 0.5	~3.0
$\langle v_F \rangle$, 10^{-5} m/s	3.2	3.2	4.2	3.8
$\langle e_F \rangle$, eV	0.24	0.24	0.36	0.25
$\langle \nu_F \rangle$, 10^{-5} m/s	2.1	2.1	2.6	2.5

of $NbSe_3$ have unambiguously shown that the T_1 transition primarily affects type III chains and the T_2 transition type I chains. The b^* component of the interband nesting for type I chains and that for type III chains, calculated from Figures 7 and 8, are $\sim 0.25b^*$ for both $NbSe_3$ and TaS_3, in good agreement with the experimental values. The spatial scale of the 1D CDW pretransitional fluctuations along the chain direction, observed in a X-ray diffuse scattering experiment, for example, is measured by the so-called coherence length $\xi_\parallel$,[19,29] which becomes infinite when a long-range order sets in throughout the lattice at the 3D CDW ordering temperature. As shown in the Appendix, in the 1D fluctuation regime and for noninteracting electrons (a reasonable assumption for $NbSe_3$[22]), $\xi_\parallel$ is a function of temperature T, the Fermi level e_F (measured from the bottom of a band), and the Fermi velocity v_F (i.e., the slope of the $e(k)$ vs k plot at the Fermi vector $\mathbf{k}_F$). As shown in Table III, the X-ray diffuse scattering measured values[17,19] of $\xi_\parallel$ are well explained by the present band calculations for $\mathbf{q}_1$ and $\mathbf{q}_2$ CDW's of both $NbSe_3$ and TaS_3.

In $NbSe_3$ or TaS_3, the two Fermi surfaces derived from type III chains are less warped than those derived from type I chains. Flatter Fermi surfaces lead to a better nesting and thus a stronger

(19) Pouget, J. P.; Comes, R. In *Charge Density Waves in Solids*; Gork'ov, L. P., Gruner, G., Eds.; Modern Problems in Condensed Matter Science Series; Elsevier: Amsterdam, The Netherlands; in press.
(20) Ong, N. P.; Monceau, P. *Phys. Rev. B* **1977**, *16*, 3443.

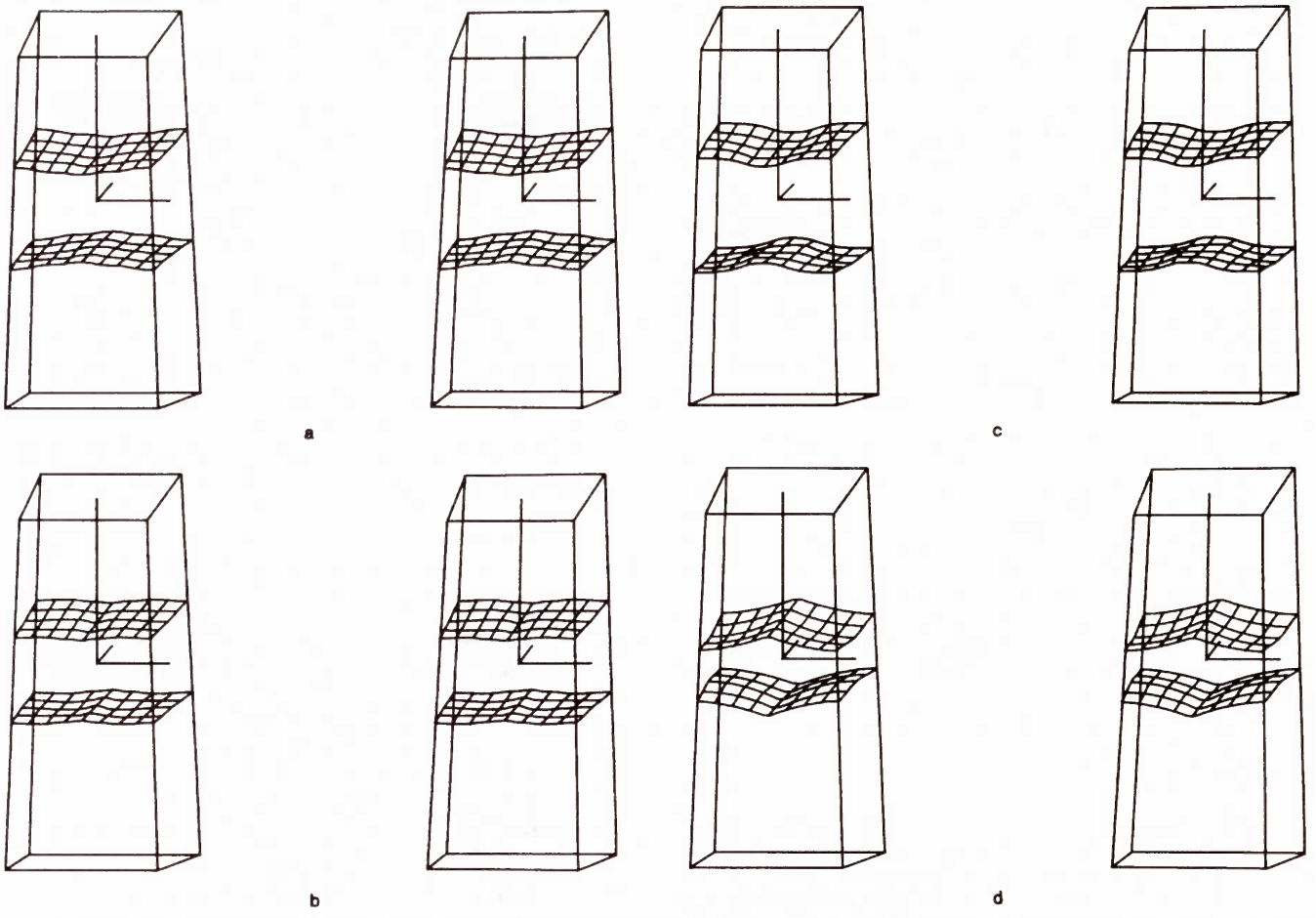

Figure 8. Fermi surfaces of TaS_3 calculated for the (a) second, (b) third, (c) first, and (d) fourth partially filled bands of Figure 6 (on going from Y to Γ at the Fermi level). The a^*, b^*, and c^* axes form a right-handed coordinate system, and the b^* axis corresponds to the vertical axis.

tendency toward a CDW instability through a stronger divergence at $2\mathbf{k}_F$ of the electronic polarizability.[21] Therefore, Fermi surface nesting would be better in TaS_3 than in NbSe3. In both TaS_3 and $NbSe_3$, nesting of the Fermi surfaces of type III chains would be better compared with that for type I chains. It is interesting to note that a better nesting appears to lead a higher 3D ordering temperature (T_c). Namely, each CDW of TaS_3 occurs at a higher temperature than the corresponding one of $NbSe_3$, and the CDW of type III chains occurs at a higher temperature with respect to that of type I chains in both $NbSe_3$ and TaS_3. As in quasi-1D conductors, the 3D ordering temperature depends on the divergence at $2\mathbf{k}_F$ of the electronic polarizability and also on the electron–phonon and CDW Coulomb interchain couplings.[22] The qualitative correspondence between the T_c and the degree of nesting of the Fermi surface is difficult to understand, except if the couplings are quite similar for both kinds of chains and materials. In both $NbSe_3$ and TaS_3, the Fermi surfaces of type I chains are more warped than those of type III chains due in part to the fact that type I chains interact strongly with type II chains to form the quadruple chains **3**. Therefore, the short intra- and interlayer contacts should have stronger effects on the type I chain CDW instability than on the type III chain CDW instability. This is consistent with the observation[23] that the pressure-induced change in the CDW transition temperature is greater for the $\mathbf{q}_2$ CDW than for the $\mathbf{q}_1$ CDW in $NbSe_3$. The good Fermi surface nesting of TaS_3 is responsible for its semiconducting property below T_2, and the poorer Fermi surface nesting of $NbSe_3$ explains its metallic property below T_2.

Coupling between CDW's

The two main mechanisms of coupling between CDW's are the interchain tunneling and/or the Coulomb interaction.[22] In the former mechanism, the transverse components of the wave vector of the CDW are fixed by the best nesting condition of the Fermi surface. In the latter one, it is fixed by the minimization of Coulomb interactions between individual CDW's. Because of the irregular shape of the Fermi surface, especially for $NbSe_3$ (Figure 7), it is difficult to discuss quantitatively the tunneling mechanism without a precise calculation of the electronic polarizability as a function of the tridimensional nesting wave vector. However, some general considerations can be made for the Coulomb coupling mechanism.

In classical terms, it may be considered that CDW modulations occur in individual I-prismatic chains. Thus, it is of interest to examine how such CDW modulations on individual chains interact within a pair of double-prismatic chains and also between pairs of such chains. We discuss this problem for the $\mathbf{q}_1$ CDW of $NbSe_3$, for which experimental data are available. Along the b^* axis, the position of satellite reflections of the $\mathbf{q}_1$ CDW is given by $(0, k \pm q_{b^*}, 0)$, where k is an odd integer.[24] From the latter observation it was deduced[24] that, within each pair of type III chains, the CDW modulations are arranged out-of-phase as illustrated in Figure 9a. This out-of-phase arrangement leads to the optimum Coulomb interactions between the CDW's.[22] Pairs of type III chains

(21) (a) Hasegawa, Y.; Fukuyama, H. *J. Phys. Soc. Jpn.* **1986**, *55*, 3978. (b) Montambaux, G. *Phys. Rev. B* **1988**, *38*, 4788.

(22) Barisic, S. In *Electronic Properties of Inorganic Quasi-One-Dimensional Materials*; Monceau, P., Ed.; Reidel: Dordrecht, The Netherlands, 1985; Part I, p 1.

(23) (a) Chaussy, J.; Haen, P.; Lasjaunias, J. C.; Monceau, P.; Waysand, G.; Waintal, A.; Meerschaut, A.; Molinie, P.; Rouxel, J. *Solid State Commun.* **1976**, *20*, 759. (b) Briggs, A.; Monceau, P.; Nunez-Regueiro, M.; Peyrard, J.; Ribault, M.; Richard, J. *J. Phys. C: Solid State Phys.* **1980**, *13*, 2117.

(24) Moudden, A. H.; Girault, S.; Pouget, J. P.; Monceau, P.; Levy, F. In *Abstracts of the 2nd European Workshop on CDW (Aussois 87)*; CNRS: Aussois, France, 1987; p 74.

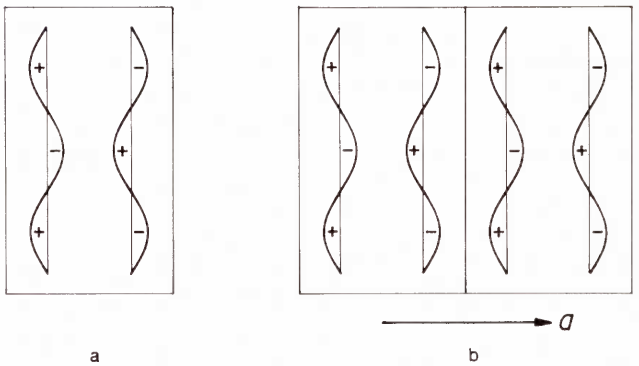

Figure 9. Out-of-phase arrangements of CDW modulations on individual I-prismatic chains (represented by wavy lines) in (a) a pair of type III chains and (b) adjacent pairs of type III chains along the *a* direction. The + and − signs of each wave line refer to the regions of excess positive and negative charges, respectively, of the CDW modulation with respect to the charge distribution of the normal metallic state.

contribute two partially filled bands, which represent bonding and antibonding between type III chains in each pair. It was found[25] that lattice vibrational modes producing an out-of-phase arrangement of CDW modulations in each pair of chains can only induce a (first-order) electron–phonon coupling that relates the bonding to the antibonding band. This is consistent with the interband nesting mechanism considered in the previous section. A similar situation was found to occur in the CDW formation of $K_{0.3}MoO_3$.[26] Thus, it appears that the electron–phonon coupling between electronic states of different symmetry (i.e., bonding and antibonding), built from like orbitals belonging to pairs of chains with strong interaction, leads to the formation of CDW's with favorable Coulomb interactions between individual chains.

The uniform ordering of the $\mathbf{q}_1$ CDW along the *a* direction (i.e., the a^* component of $\mathbf{q}_1$ is zero) can be understood as a result of optimizing the Coulomb interactions between neighboring pairs of type III chains along the *a* direction as illustrated in Figure 9b. Since pairs of type III chains are farther separated along the *c* than along the a^* direction, the CDW coupling should be weaker along the *c* direction. In fact, the CDW transverse coherence lengths are observed to be twice greater along the a^* than along the *c* direction (i.e., $\xi_{a^*} \simeq 2\xi_c$].[19] The c^* component of the $\mathbf{q}_1$ CDW is zero as well, which must be due to the indirect interactions that occur between pairs of type III chains via the intervening quadruple chain units **3** along the *c* direction. In the quadruple chain units **3**, type I chains are "wrapped" by type II chains. The latter chains may play an important role as a polarizing medium for Coulomb interactions between CDW's on type I and type III chains, because they contribute to electronic states in the vicinity of the Fermi energy.

Concluding Remarks

In the present study, we have calculated the tight-binding band electronic structures and the Fermi surfaces of three layered trichalcogenides $NbSe_3$, TaS_3, and $TaSe_3$ and have examined how their electronic structures near the Fermi level are related to the crystal structures. In these trichalcogenides MX_3, the broken X–X bonds of the E-prismatic chains are primarily responsible for the highest lying chalcogen p-block bands that overlap with the bottom of the z^2-block bands. Thus, with a zero d-electron count on the metal, $TaSe_3$ becomes semimetallic. With a nonzero d-electron count on the metal,the Fermi level of $NbSe_3$ or TaS_3 occurs in the z^2-block bands, slightly above the region where the chalcogen p-block band top overlaps with the z^2-block band bottom. Thus, $NbSe_3$ and TaS_3 acquire primarily 1D metallic character, but they deviate from purely 1D character due to the short intra- and interlayer X···X contacts. Deviation from 1D character is stronger for $NbSe_3$ than for TaS_3, since such X···X contacts provide a stronger overlap for X = Se compared with the case of X = S. Consequently, the Fermi surfaces of $NbSe_3$ are more warped than those of TaS_3 so that the Fermi surface nesting is better for TaS_3. This explains why TaS_3 becomes semiconducting but $NbSe_3$ remains metallic after the $\mathbf{q}_1$ and $\mathbf{q}_2$ CDW transitions. The physical parameters of the $\mathbf{q}_1$ and $\mathbf{q}_2$ CDW's in $NbSe_3$ and TaS_3 derived from our calculations are in excellent agreement with the experimentally derived values.

Acknowledgment. This work was supported by NATO, Scientific Affairs Division, and also by DOE, Office of Basic Energy Sciences, Division of Materials Science, under Grant DE-FG05-86ER 45259. J.P.P. acknowledges useful discussions with S. Girault, G. Montambaux, R. Moret, and A. H. Moudden.

Appendix

In the 1D regime of fluctuation of the amplitude of the order parameter, where the CDW response function at $2\mathbf{k}_F$ for noninteracting electrons behaves as a function of temperature as log (T/T_{eff}),[27] the CDW coherence length $\xi_\parallel$ measured in an X-ray diffuse scattering experiment[29] is given by[19]

$$\xi_\parallel^{-1} = \xi_e^{-1}[\log (T/T_{eff})]^{1/2} \quad (1)$$

where

$$\xi_e^{-1} = \xi_0^{-1}[\log (A/T)]^{1/2} \quad (2)$$

with

$$\xi_0 = \frac{h}{2\sqrt{2}\pi^2 k_B T} v_F \quad (3)$$

The term log (A/T) of eq 2 represents the temperature-dependent part of the $2\mathbf{k}_F$ electronic polarizability. From (2) and (3) the effective Fermi velocity v_F can be defined as

$$v_F = v_F/[\log (A/T)]^{1/2} \quad (4)$$

Previous studies on the temperature dependence of the CDW response in $K_{0.3}MoO_3$ and $NbSe_3$ ($\mathbf{q}_1$ CDW) showed that $T_{eff} \cong 0.93T_c$,[19] where T_c refers to the 3D CDW ordering temperature. Thus, from the experimental measurements of $\xi_\parallel$ and T_c, ξ_e and v_F can be deduced by using (1)–(3). These values obtained from the room-temperature data[19] for the $\mathbf{q}_1$ and $\mathbf{q}_2$ CDW's of $NbSe_3$ and TaS_3 are summarized in Table III.

The coefficient A of eq 2 is given by[28]

$$A = \frac{\alpha e_F}{k_B} \quad (5)$$

where k_B is the Boltzmann constant, e_F is the Fermi level (measured from the bottom of the band), and α is a coefficient which depends upon the form of the density of states in the energy range of several k_BT around e_F and which is generally between 1[21] and 4.5.[28] Since the e_F and v_F values of $NbSe_3$ and TaS_3 can be obtained from their calculated band electronic structures (Figures 5 and 6), the effective Fermi velocities v_F can also be calculated from (4). The $\langle v_F \rangle$ and $\langle e_F \rangle$ values listed in Table III are the average values calculated from each pair of bands associated with the $\mathbf{q}_1$ and $\mathbf{q}_2$ CDW's. The $\langle v_F \rangle$ values of Table III are the v_F values obtained from (4) at room temperature for $\alpha = 1$. These $\langle v_F \rangle$ values are not greatly affected by α. (For example, they are reduced by 10 and 20% for $\alpha = 2$ and 4, respectively.) It is clear from Table III that, within uncertainties inherent in our estimation, the calculated (i.e., $\langle v_F \rangle$) and the experimental (i.e., $\langle v_F \rangle$) values of the effective Fermi velocities are in excellent agreement.

Registry No. $NbSe_3$, 12034-78-5; TaS_3, 12138-12-4; $TaSe_3$, 12039-57-5.

(25) Noguera, C. *J. Phys. C: Solid State Phys.* **1986**, *19*, 2161.
(26) Pouget, J. P.; Girault, S.; Moudden, A. H.; Hennion, B.; Escribe-Filippini, C.; Sato, M. *Phys. Scr.* **1989**, *T25*, 58.
(27) Schulz, H. J. In *Low Dimensional Conductors and Superconductors*; NATO ASI B155; Jerome, D., Caron, L. G., Eds.; Plenum Press: New York, 1987; p 95.
(28) Horowitz, B.; Gutfreund, H.; Weger, M. *Phys. Rev. B* **1975**, *12*, 1975.
(29) Pouget, J. P. In *Low Dimensional Electronic Properties of Molybdenum Bronzes and Oxides*; Schlenker, C., Ed.; Kluwer Academic Publishers: Dordrecht, The Netherlands, 1989; p 87.